Supplementary Information

Reconstructing two-dimensional defects in CuO nanowires for efficient CO_2 electroreduction to ethylene

Jianfang Zhang,[ab] Zhengyuan Li,[b] Shuai Xia,[c] Tianyu Zhang,[b] Yan Wang,[cd*] Yucheng Wu,[cd*] and Jingjie Wu [b*]

[a]School of Instrument Science and Opto-electronics Engineering, Hefei University of Technology, Hefei 230009, China.

[b]Department of Chemical and Environmental Engineering, University of Cincinnati, Cincinnati, OH 45221, United States.

[c]School of Materials Science and Engineering, Hefei University of Technology, Hefei 230009, China.

[d]China International S&T Cooperation Base for Advanced Energy and Environmental Materials & Anhui Provincial International S&T Cooperation Base for Advanced Energy Materials, Hefei University of Technology, Hefei 230009, China.

*Corresponding authors：

Dr. Yan Wang, E-mail: stone@hfut.edu.cn.

Prof. Yucheng Wu, E-mail: ycwu@hfut.edu.cn.

Prof. Jingjie Wu, E-mail: jingjie.wu@uc.edu

Experimental section

Synthesis of CuO samples

The CuO samples were prepared by microwave synthesis method. First, 10 mmol $CuCl_2$ were dissolved into 10 ml DI water to form a uniform solution. Second, the $CuCl_2$ solution was added into 30 ml of 3 M KOH solution with additional 10 ml ethanol under continuous stirring for 10 min. Then, the resultant solution was placed in the microwave oven and heated for 30 min. Lastly, the obtained samples were washed, centrifuged, and dried in air. Four different microwave powers of 200, 300, 400 and 500 W were selected to synthesize CuO samples, and the corresponding samples were denoted as CuO-1, CuO-2, CuO-3, and CuO-4, respectively.

Characterizations

The morphology of CuO samples was characterized by a SU8020 scanning electron microscopy (SEM) and a JEM-2100F transmission electron microscopy (TEM). X-ray diffusion (XRD) tests were carried out on a PANalytical X-Pert PRO MPD with Cu-target X-ray source. X-ray photoelectron spectra (XPS) data were collected on a ESCAL AB250Xi spectrometer using Al Kα X-ray source. In situ Raman spectra were measured on a LabRAM HR Evolution Raman spectrometer with a 633 nm laser equipped with a gas-fed flow cell (Gaossunion Technology CO., Ltd).

Preparation of electrodes

The CuO catalysts were first dispersed in a mixture solution containing 10 ml of DI water, 10 ml of isopropyl alcohol, and 30 μl of Nafion ionomer solution (Sigma; 5 wt %). The CuO solution was then sonicated for 30 min to form catalyst ink. The gas diffusion electrodes (GDEs) were prepared by spraying the catalyst ink onto a 2 × 2 cm^2 carbon paper with a microporous carbon layer (SGL 34BC). The loading of catalysts was controlled to about 0.5 mg cm^{-2}. Ni foam was pressed on the carbon paper as an anode electrode.

Electrochemical measurements

The electrochemical CO_2 reduction reaction measurements were conducted using a flow cell system under constant cell voltage electrolysis controlled by a Gamry electrochemical workstation. The as-prepared CuO-GDEs were employed as the

cathode. A polytetrafluoroethylene (PTFE) buffer layer with a 1 cm^2 window was attached to the cathode. 1.0 M KOH aqueous solution was pumped to the cathodic and anodic PTFE buffer layer compartments at a rate of 1.0 ml min^{-1}. The cathodic and anodic compartments were separated by an anion exchange membrane (Fumasep FAA-3-PK-75). CO_2 gas was continuously supplied to the cathode through a serpentine bipolar plate with a flow rate of 20.0 sccm. The gas from the outlet of the flow cell was mixed with Ar stream at a fixed flow rate of 10 sccm before looping to the gas chromatography. The outlet CO_2 flow rate was calibrated by the Ar stream. All potentials were converted to a reversible hydrogen electrode (RHE) scale with manual iR_s compensation: $E_{RHE} = E_{Ag/AgCl\ (saturated\ KCl)} + 0.059 \times pH + 0.197 - iR_s$. The R_s was determined by potentiostatic electrochemical impedance spectroscopy (EIS) measurement under an open circuit potential at frequencies ranging from 100 kHz to 0.1 Hz. Before the electrocatalytic test, the cathode was pretreated by cyclic voltammetry from -0.5 to -1.0 V vs. RHE for 3 cycles. The electrochemical active surface area (ECSA) of the electrodes was proportional to the double-layer capacitance (C_{dl}) value. The C_{dl} of each electrode was estimated from the cyclic voltammetric curves ranged from 0.2 to 0.3 V vs. RHE with various scan rates from 10 to 200 mV s^{-1}.

Product analysis

The gaseous products were detected by on-line gas chromatography (GC 7890B, Agilent) equipped with a thermal conductivity detector (TCD) and a flame ionization detector (FID). High purity helium (He) gases were used as the carrier gas. The outlet gas stream was injected into GC after CO_2 electrocatalysis for 5 min at each potential. The molar percentage of gas product was obtained from the ratio of GC peak area between the specific gas product and CO_2 based on the calibration curves (TCD for H_2, CO_2, and CO; FID for CH_4, C_2H_4, and C_2H_6). The liquid products were quantified by ^1H NMR (Bruker AV 400 MHz spectrometer). The liquid product concentration was calculated referred to the concentration of internal standard solution based on the NMR peak integral areas and calibration curves. To prepare the NMR samples, 500 μl of the collected electrolyte was mixed with 100 μl D_2O solution containing 5 mM of 3-(trimethylsilyl)propionic-2,2,3,3-d_4 acid sodium salt (TSP).

The partial current (I_x) and the Faradaic efficiency (FE_x) of a specific gas product x were calculated by the following equation:

$$I_x = \frac{\frac{A_x}{A_{CO_2}}}{\frac{A_x^*}{A_{CO_2}^*}} \times C_x^* \times \left(\frac{\frac{A_{CO_2}}{A_{Ar}} - b}{a} \times v_{Ar}\right) \times P \times \frac{n_x F}{RT}$$

$$FE_x = I_x / I_{total}$$

Where the A_x, A_{CO2} and A_{Ar} represent the peak area of a specific gas product, CO_2 and Ar in the sample gas; the A_x* and A_{CO2}* represent the peak area of a specific gas product and CO_2 in the calibration gas; the C_x* represents the fraction of the specific gas referred to CO_2 in the calibration gas; the a and b are slope and intercept of the linear relationship between the A_{CO2}/A_{Ar} and v_{CO2}/v_{Ar} , respectively, from the GC calibration; v_{Ar} is the volumetric flow rate of Ar, which is 10 sccm; q is the volumetric flow rate CO_2, which is 20.0 sccm; P and T are the atmospheric pressure and temperature during test, respectively; R is the gas constant; F is the Faradaic constant; n_x is the electron transfer number for a specific gas product and I_{total} is the total current during the test.

The gross CO generation rate was defined as the summary of the production rates of C_{2+} products, CH_4, and residual CO gas product, which was calculated by the following equation:[S1]

$$j_{CO,\ generation} = j_{CO} + \frac{j_{CH4}}{4} + \frac{j_{C2H4}}{3} + \frac{j_{C2H5OH}}{3} + \frac{j_{C3H7OH}}{3} + \frac{j_{CH3OOH}}{2}$$

The electrochemical active surface area (ECSA) was obtained based on the roughness factor (RF), which can be calculated by the equation of $RF=C_{dl}/C_f$, C_{dl} is the double-layer capacitance of the CuO electrode, C_f is the double-layer capacitance of the Cu foil flat surface (35 μF cm^{-2}).[S2]

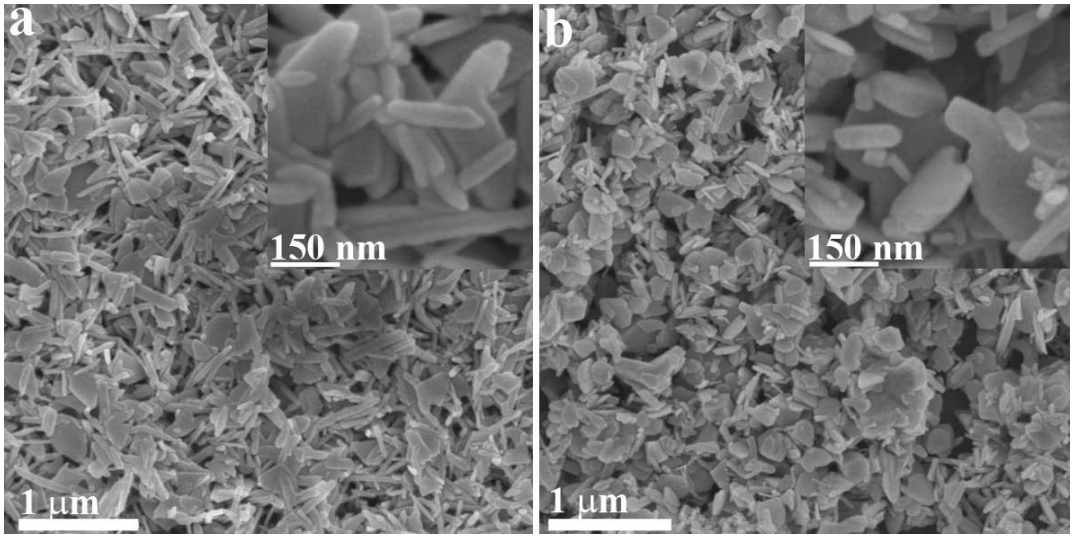

Fig. S1. SEM images of (a) CuO-2 and (b) CuO-3 samples.

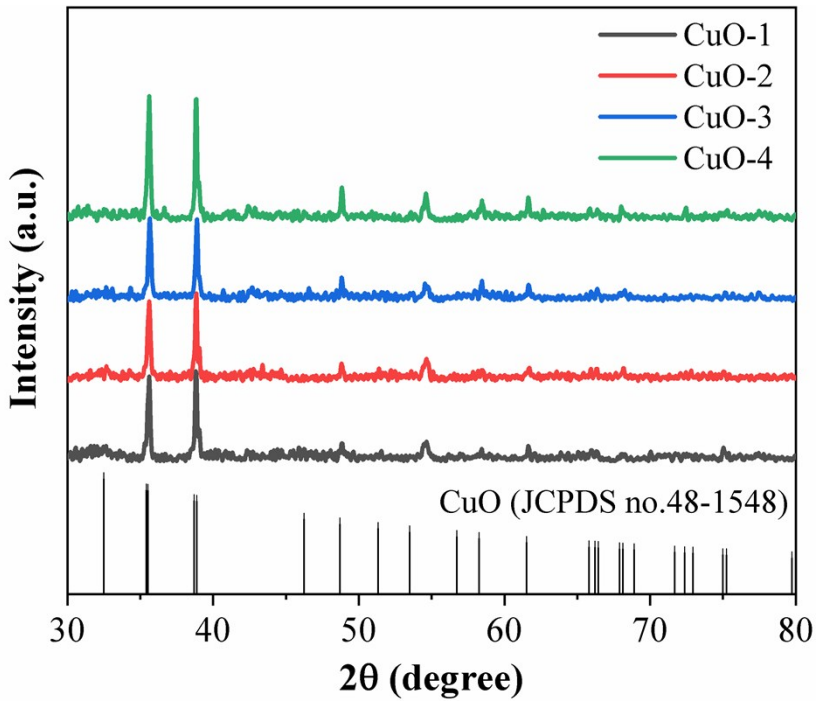

Fig. S2. XRD patterns of different CuO samples.

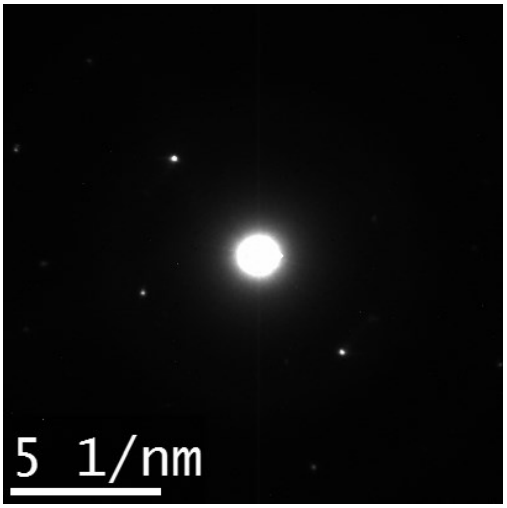

Fig. S3. The selective electron diffraction pattern of CuO-1 sample.

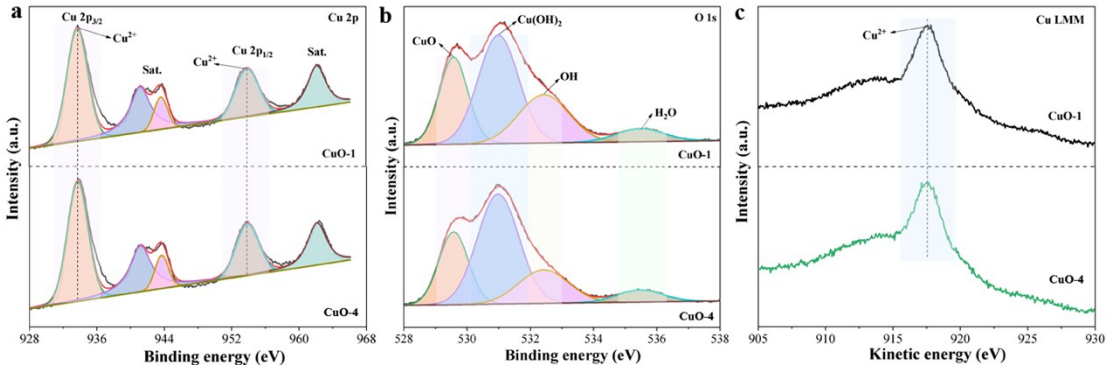

Fig. S4. XPS spectra of CuO-1 and CuO-4: (a) Cu 2p, (b) O 1s, (c) Cu LMM.

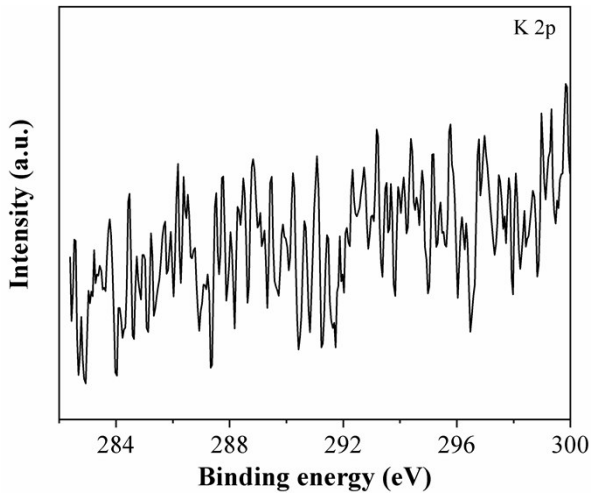

Fig. S5. XPS spectrum of K 2p for CuO-1 sample.

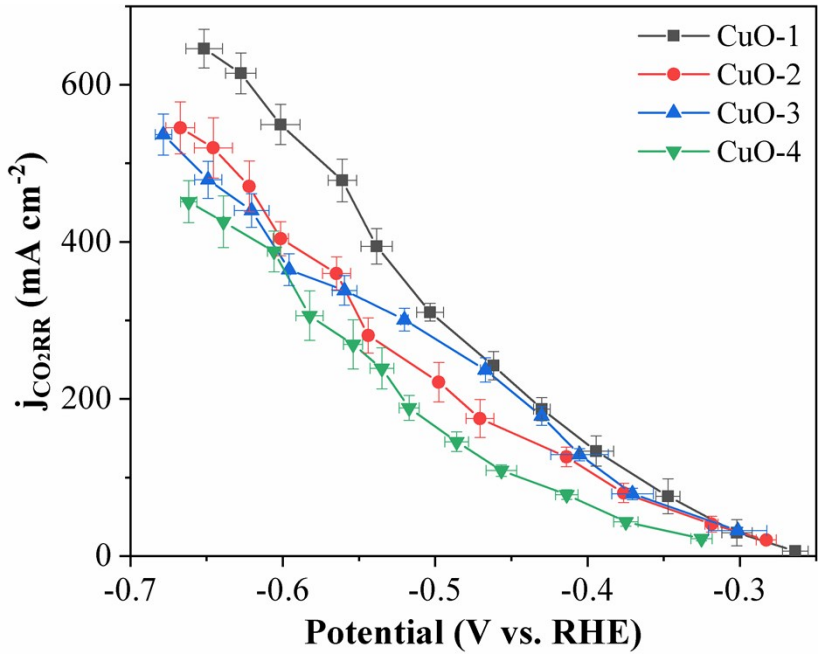

Fig. S6. CO_2RR current densities of different CuO electrodes.

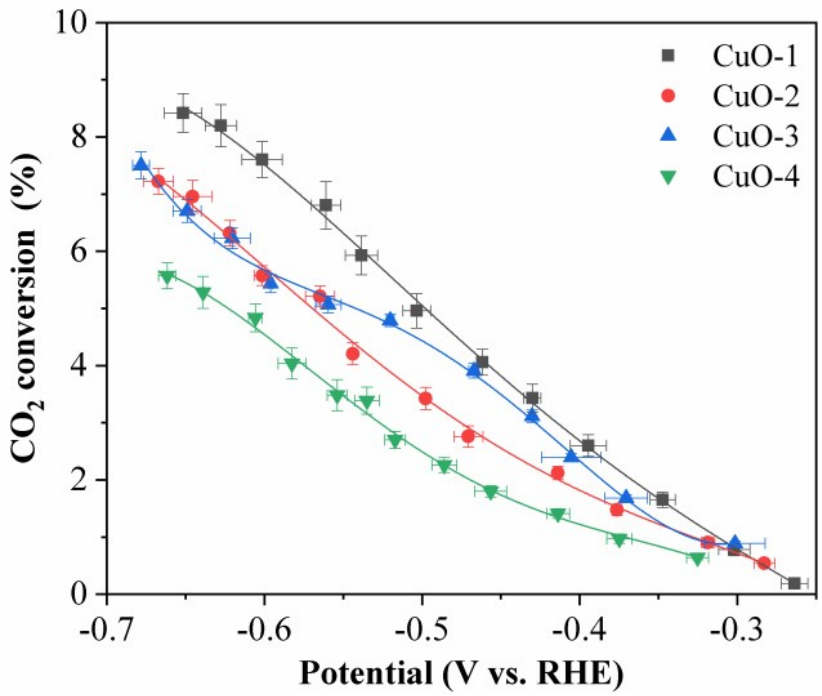

Fig. S7. CO_2 conversion over the different CuO catalysts. The CO_2 conversion is referred to the ratio of consumed CO_2 by the electrochemical reduction to supplied CO_2.

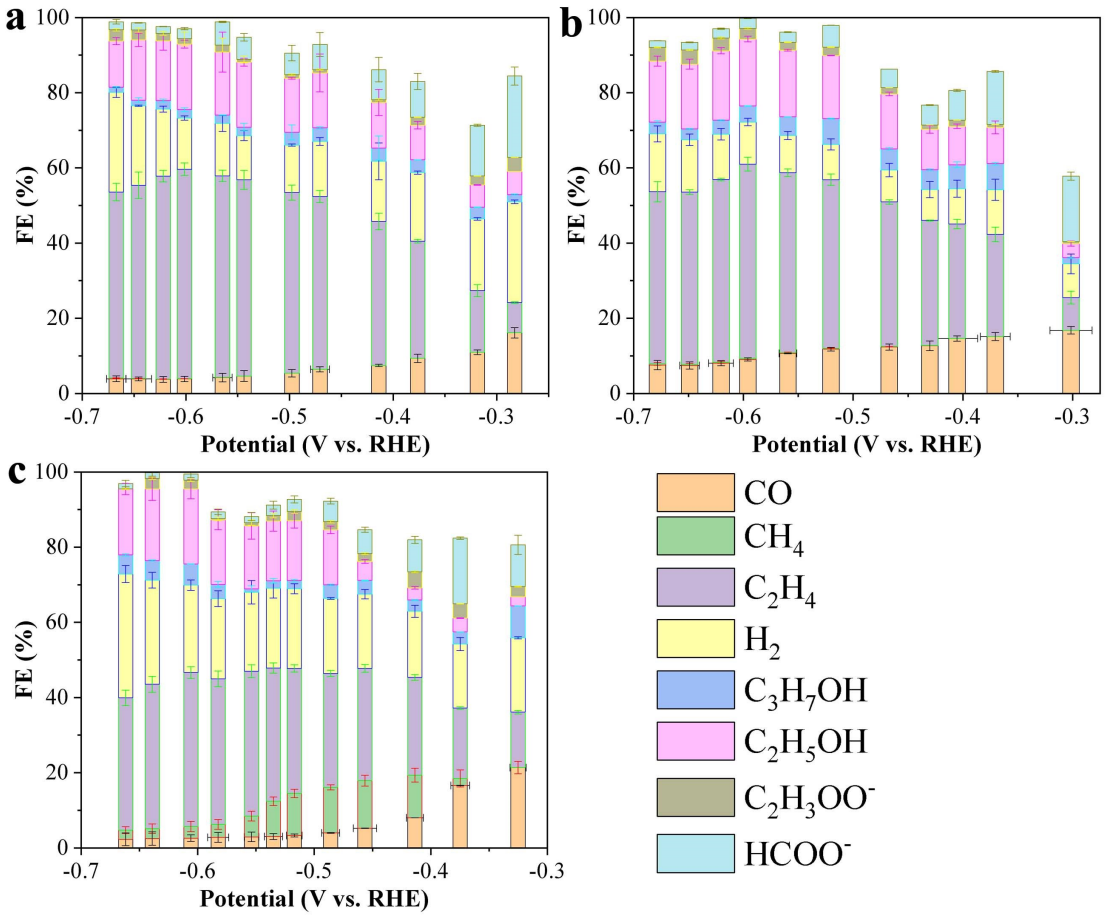

Fig. S8. Faradaic efficiencies of all CO_2 reduction products for (a) CuO-2, (b) CuO-3, and (c) CuO-4 electrodes.

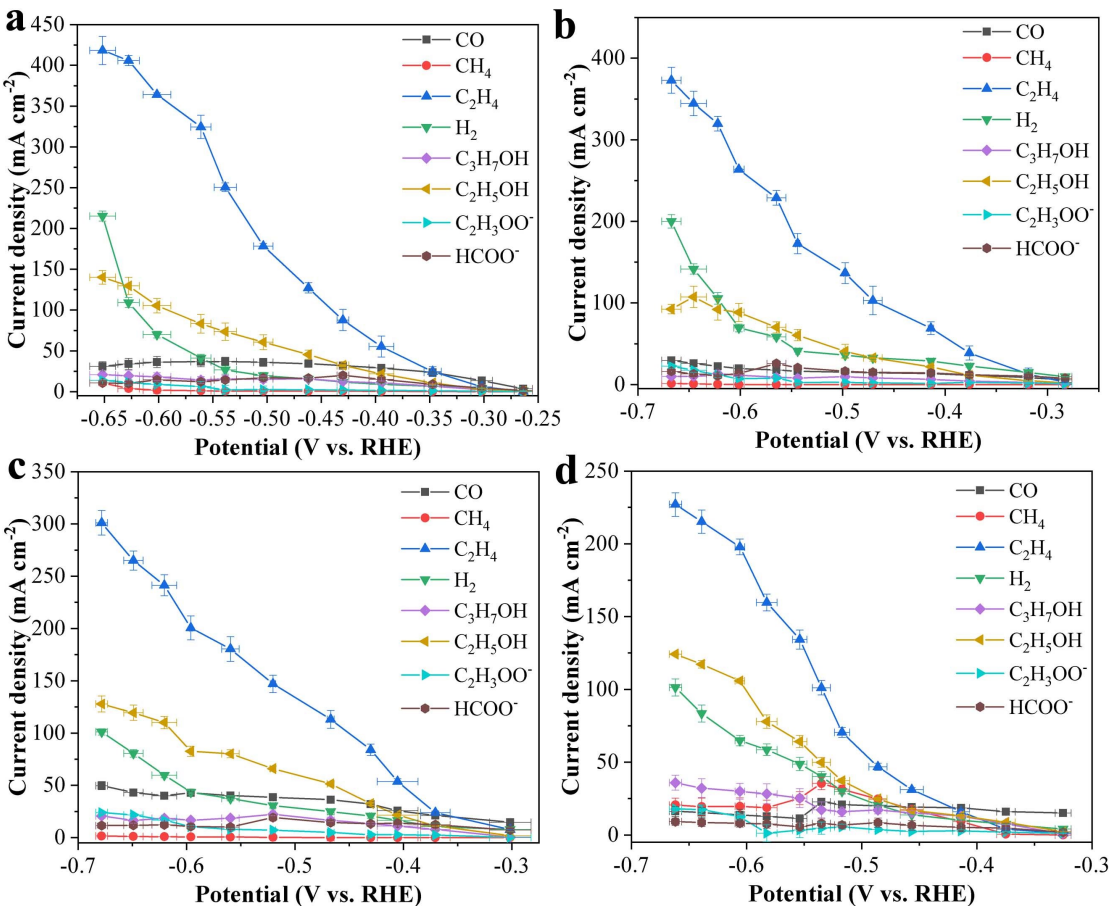

Fig. S9. Partial current densities of all CO_2 reduction products for (a) CuO-1, (b) CuO-2, (c) CuO-3, and (d) CuO-4 electrodes.

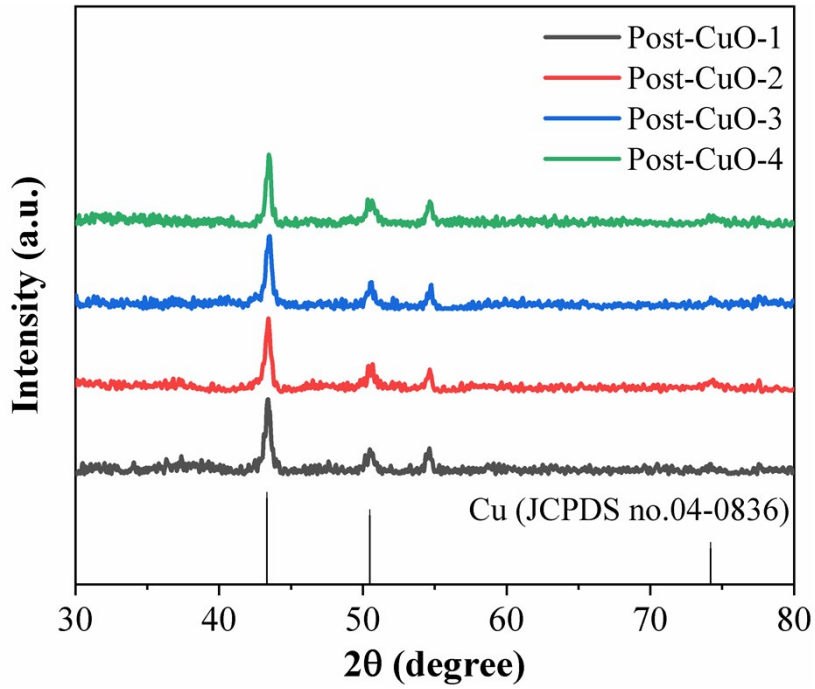

Fig. S10. XRD patterns of the different spent CuO electrodes after CO_2RR.

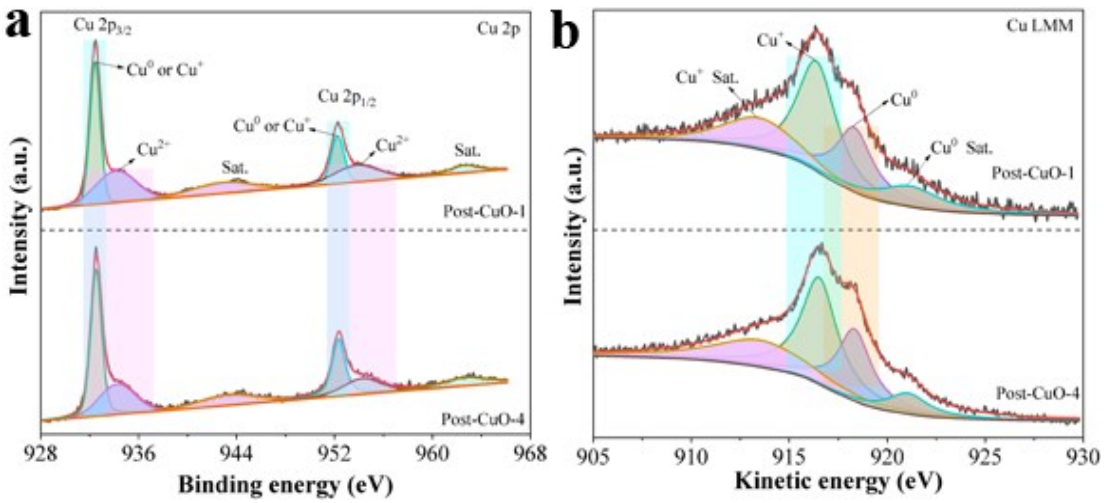

Fig. S11. XPS spectra of spent CuO-1 and CuO-4 after CO_2RR: (a) Cu 2p, (b) Cu LMM.

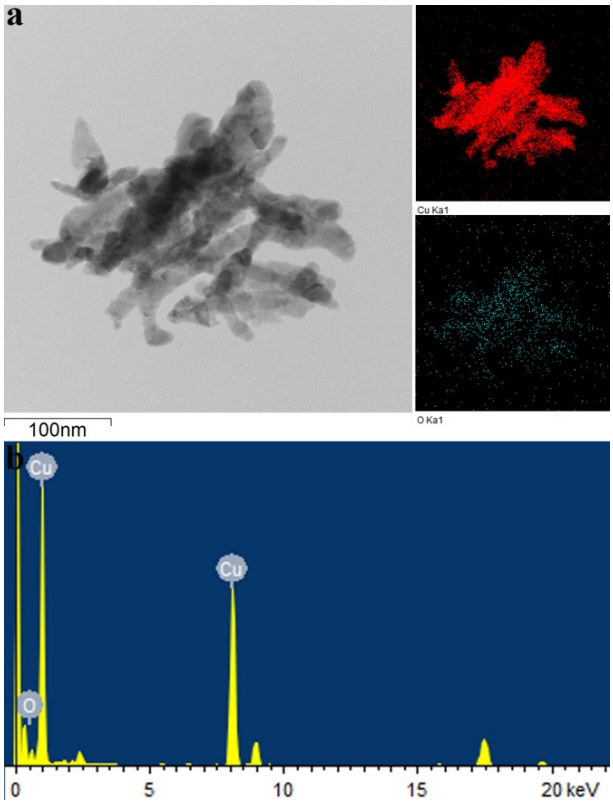

Fig. S12. (a) EDS mapping and (b) EDX spectrum of post CuO-1 after CO_2RR.

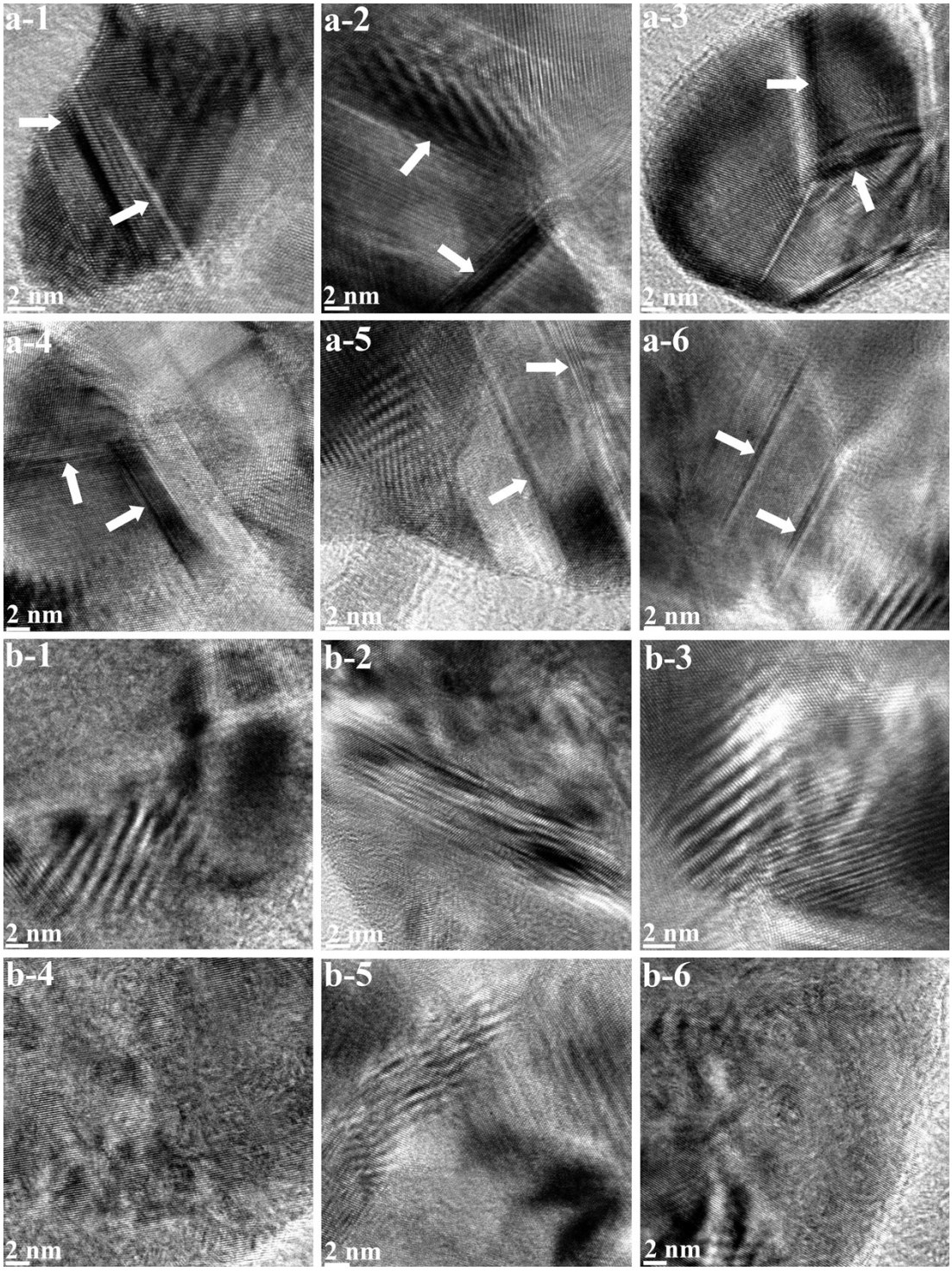

Fig. S13. HRTEM images of (a1-6) spent CuO-1 electrode and (b1-6) spent CuO-4 electrode after CO_2RR.

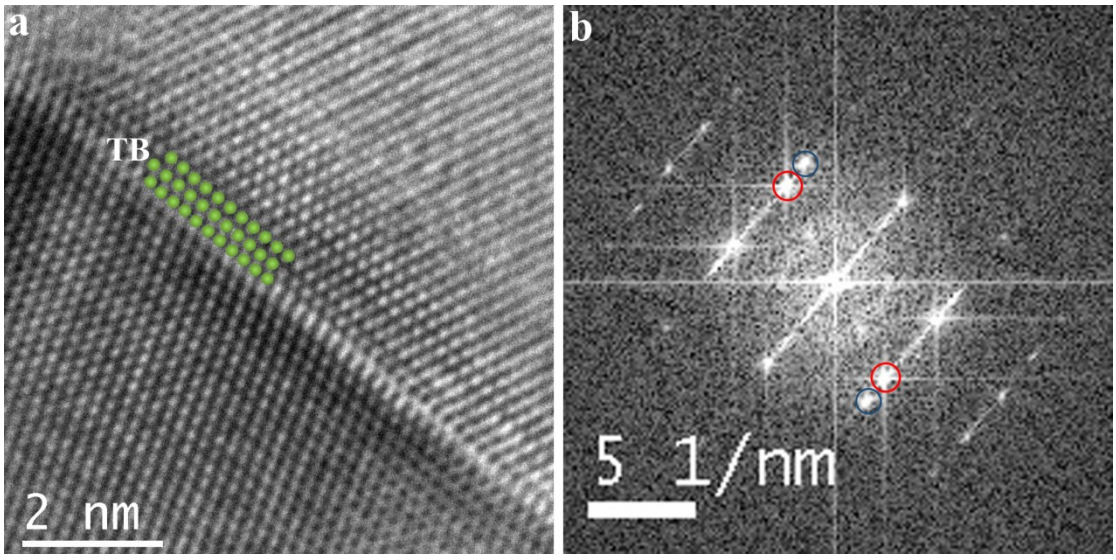

Fig. S14. (a) HRTEM image of post CuO-1 after CO_2 reduction, (b) the corresponding FFT pattern.

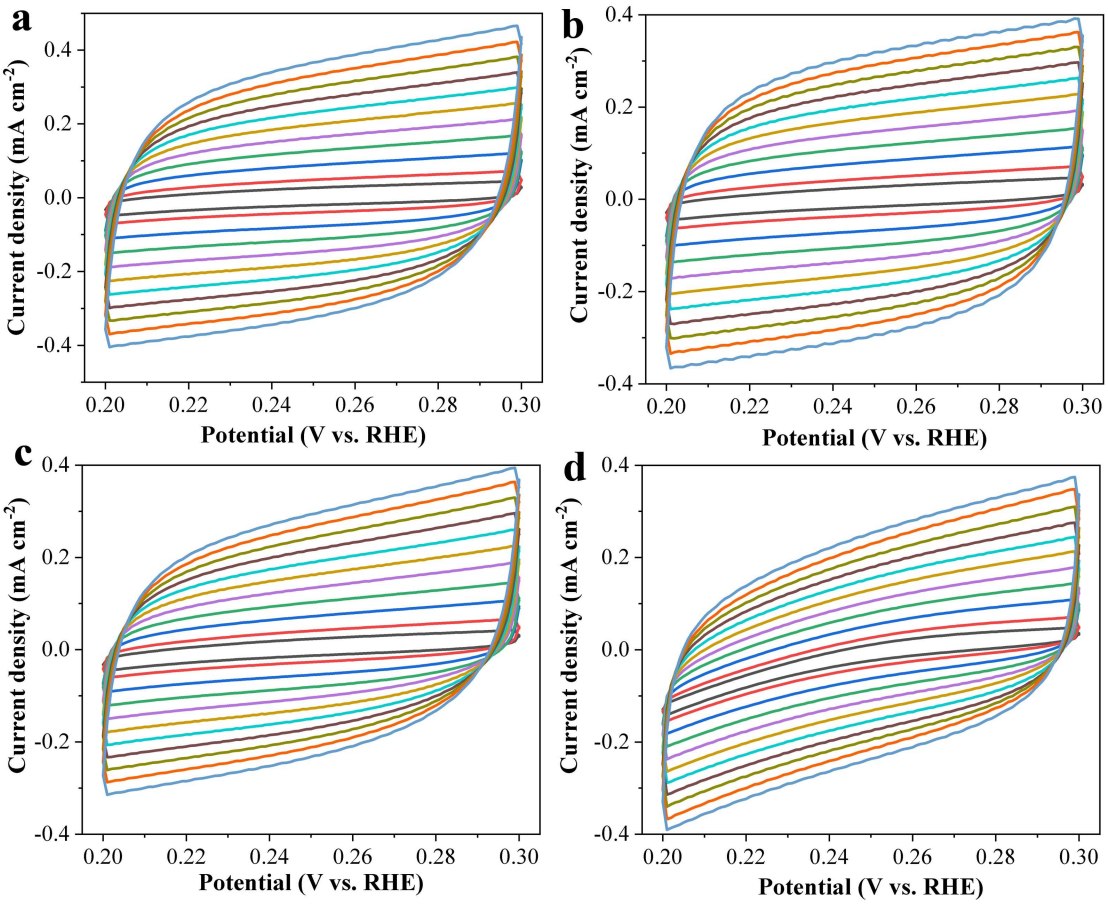

Fig. S15. Cyclic voltammetry curves of different CuO electrodes at scan rates of 10, 20, 40, 60, 80, 100, 120, 140, 160, 180, and 200 mV s^{-1}. (a) CuO-1, (b) CuO-2, (c) CuO-3, and (d) CuO-4 electrodes.

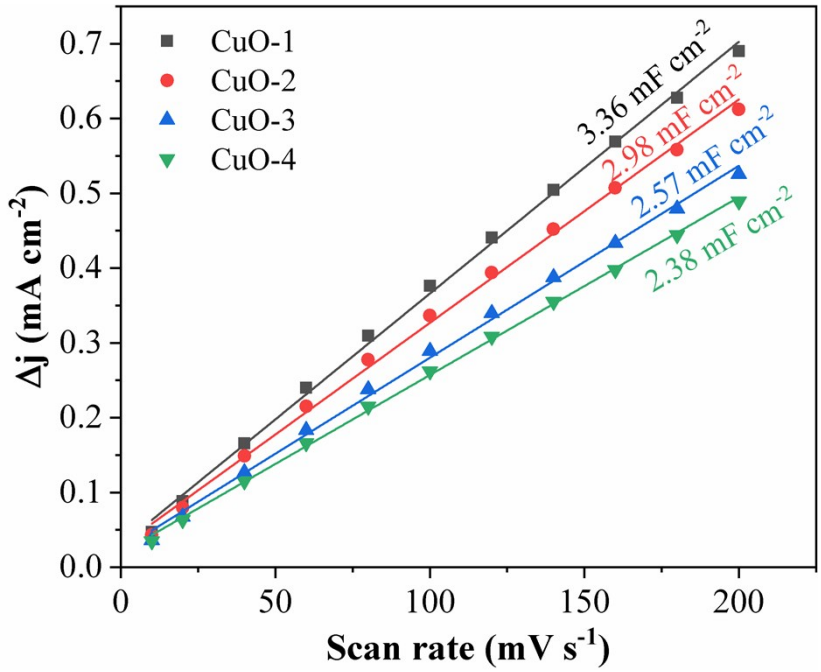

Fig. S16. The double-layer capacitances of different CuO electrodes.

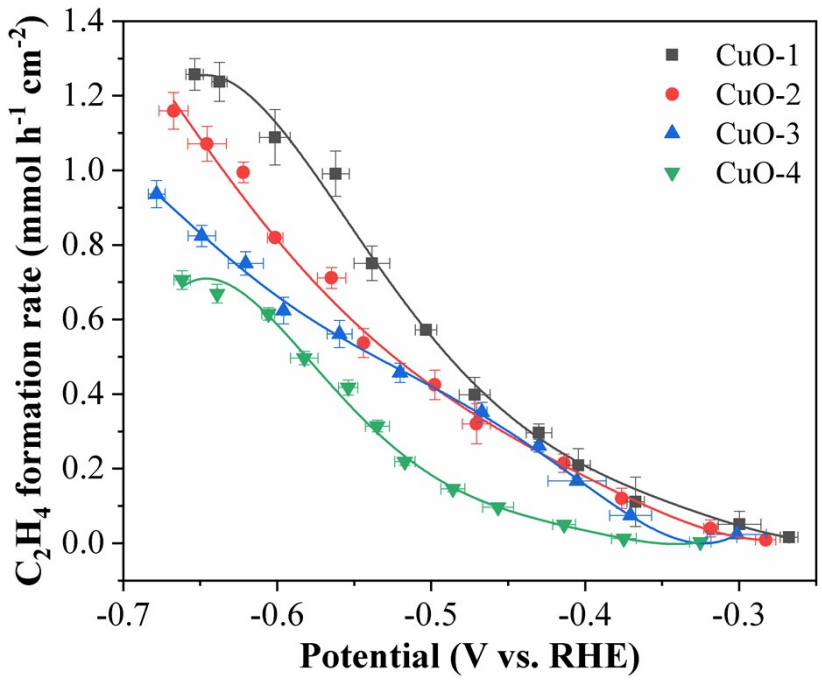

Fig. S17. C_2H_4 formation rate as a function of potential for different CuO electrodes.

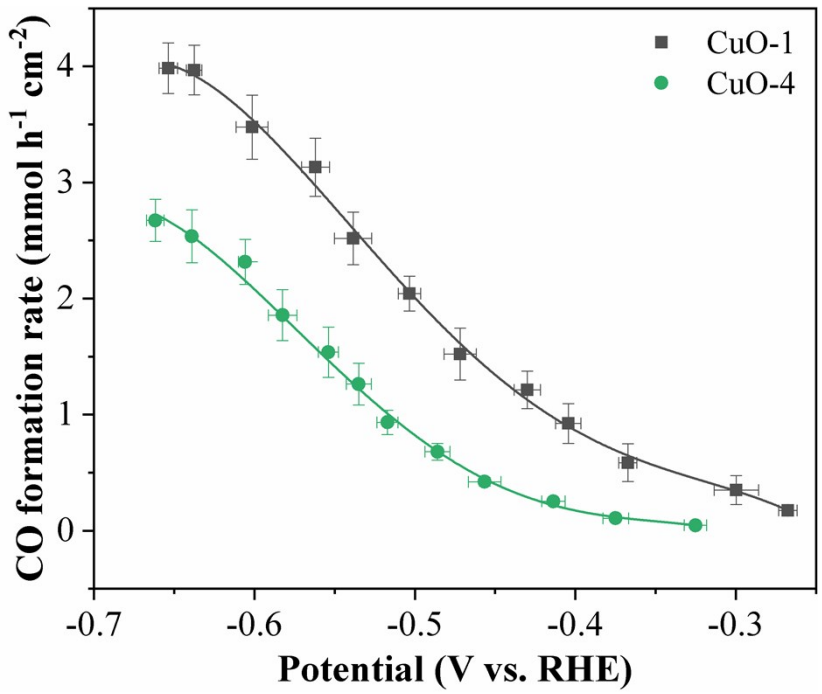

Fig. S18. CO formation rates of the CuO-1 and CuO-4 electrodes.

Table S1. Comparison of C_2H_4 production rate and Faradaic efficiency among various Cu-based catalysts.

Catalyst	electrolyte	j_{C2H4} (mA cm^{-2})	FE_{C2H4} (%)	Potential (V vs. RHE)	Ref.
CuO nanowires	1 M KOH	325	62	-0.56	This work
CuAg alloy	1 M KOH	~180	60	-0.70	S3
Cu-Al alloy	1 M KOH	400	80%	-1.50	S4
Cu–polyamine	1 M KOH	312	72	-0.97	S5
Molecular functionalized Cu	1 M $KHCO_3$	232	72	-0.83	S6
Cu nanowires	0.1 M $KHCO_3$	-	20.3	-1.10	S7
plasma-copper	0.1 M $KHCO_3$	-	60	-0.90	S8
plasma-copper	0.1 M $KHCO_3$	~15	~45	-1.00	S9
CuO_x–Vo	0.1 M $KHCO_3$	-	63	-1.40	S10
AN-Cu	0.1 M $KHCO_3$	7.3	38.1	-1.08	S11
SD-Cu NPs	0.1 M $KHCO_3$	2.0	52.43	-0.99	S12
PISG-3	1 M KOH	143	61.1	-0.90	S13
Cu-SiO_x	0.1 M $KHCO_3$	215	65	-	S14
Nanodefective Cu Nanosheets	0.1 M K_2SO_4	~60	83.2	-1.18	S15

References:

S1. T. Zhang, Z. Li, J. Zhang and J. Wu, *J. Catal.*, 2020, **387**, 163-169.

S2. Q. Zhu, X. Sun, D. Yang, J. Ma, X. Kang, L. Zheng, J. Zhang, Z. Wu and B. Han, *Nat. Commun.*, 2019, **10**, 3851.

S3. T. T. H. Hoang, S. Verma, S. Ma, T. T. Fister, J. Timoshenko, A. I. Frenkel, P. J. A. Kenis and A. A. Gewirth, *J. Am. Chem. Soc.*, 2018, **140**, 5791-5797.

S4. M. Zhong, K. Tran, Y. Min, C. Wang, Z. Wang, C. T. Dinh, P. De Luna, Z. Yu, A. S. Rasouli, P. Brodersen, S. Sun, O. Voznyy, C. S. Tan, M. Askerka, F. Che, M. Liu, A. Seifitokaldani, Y. Pang, S. C. Lo, A. Ip, Z. Ulissi and E. H. Sargent, *Nature*, 2020, **581**, 178-183.

S5. X. Chen, J. Chen, N. M. Alghoraibi, D. A. Henckel, R. Zhang, U. O. Nwabara, K. E. Madsen, P. J. A. Kenis, S. C. Zimmerman and A. A. Gewirth, *Nat. Catal.*, 2020, **4**, 20-27.

S6. F. Li, A. Thevenon, A. Rosas-Hernandez, Z. Wang, Y. Li, C. M. Gabardo, A. Ozden, C. T. Dinh, J. Li, Y. Wang, J. P. Edwards, Y. Xu, C. McCallum, L. Tao, Z. Q. Liang, M. Luo, X. Wang, H. Li, C. P. O'Brien, C. S. Tan, D. H. Nam, R. Quintero-Bermudez, T. T. Zhuang, Y. C. Li, Z. Han, R. D. Britt, D. Sinton, T. Agapie, J. C. Peters and E. H. Sargent, *Nature*, 2020, **577**, 509-513.

S7. M. Ma, K. Djanashvili and W. A. Smith, *Angew. Chem. Int. Ed.*, 2016, **55**, 6680-6684.

S8. H. Mistry, A. S. Varela, C. S. Bonifacio, I. Zegkinoglou, I. Sinev, Y. W. Choi, K. Kisslinger, E. A. Stach, J. C. Yang, P. Strasser and B. R. Cuenya, *Nat. Commun.*, 2016, **7**, 12123.

S9. D. Gao, I. Zegkinoglou, N. J. Divins, F. Scholten, I. Sinev, P. Grosse and B. Roldan Cuenya, *ACS Nano*, 2017, **11**, 4825-4831.

S10. Z. Gu, N. Yang, P. Han, M. Kuang, B. Mei, Z. Jiang, J. Zhong, L. Li and G. Zheng, *Small Methods*, 2018, *3*, 1800449.

S11. S. Y. Lee, H. Jung, N. K. Kim, H. S. Oh, B. K. Min and Y. J. Hwang, *J. Am. Chem. Soc.*, 2018, **140**, 8681-8689.

S12. C. Choi, T. Cheng, M. Flores Espinosa, H. Fei, X. Duan, W. A. Goddard, 3rd and Y. Huang, *Adv. Mater.*, 2019, **31**, e1805405.

S13. R.-X. Yang, Y.-R. Wang, G.-K. Gao, L. Chen, Y. Chen, S.-L. Li and Y.-Q. Lan, *Small Structures*, 2021, 2100012.

S14. J. Li, A. Ozden, M. Wan, Y. Hu, F. Li, Y. Wang, R. R. Zamani, D. Ren, Z. Wang, Y. Xu, D. H. Nam, J. Wicks, B. Chen, X. Wang, M. Luo, M. Graetzel, F. Che, E. H. Sargent and D. Sinton, *Nat. Commun.*, 2021, **12**, 2808.

S15. B. Zhang, J. Zhang, M. Hua, Q. Wan, Z. Su, X. Tan, L. Liu, F. Zhang, G. Chen, D. Tan, X. Cheng, B. Han, L. Zheng and G. Mo, *J. Am. Chem. Soc.*, 2020, **142**, 13606-13613.